# Detailed photophysical properties of a functionalized ruthenium(II) polypyridyl complex: through-space solvent effects

**Andrew C. Benniston,*[a] Philip R. Mackie,[a] Louis J. Farrugia,[a] Graeme Smith,[a] Simon J. Teat[b] and Andrew J. McLean[c]**

[a] *Department of Chemistry, Joseph Black Building, Glasgow University, Glasgow, UK G12 8QQ*
[b] *CLRC, Daresbury Laboratory, Warrington, Cheshire, UK WA4 4AD*
[c] *Department of Chemistry and Chemical Engineering, University of Paisley, Paisley Campus, Paisley, UK PA1 2BE*

***Received (in Cambridge, UK) 2nd October 2000, Accepted 18th December 2000***
***First published as an Advance Article on the web 15th February 2001***

The synthesis and detailed photophysical properties of a bis(*N*-methylene-4-pyridinium-4′-pyridine)-functionalized ruthenium(II) polypyridyl complex in solvents of varying polarity and Gutmann's donor number (DN) are reported, along with its single-crystal X-ray structure. The emission spectrum of the complex in varying solvents was also simulated and parameters, including the Huang–Rhys ($S_m$) electron-vibrational coupling constant, obtained. Reasonable correlations of the optical properties with the solvent polarity factor ($\Delta f$) and DN were observed. A difference in dipole moment between the ground and excited states of *ca.* 10 D was calculated, and a simplified potential-energy surface model proposed to explain the results. Excited state lifetimes in acetonitrile were determined over a modest temperature range of 60 K. The linear Arrhenius plot of $\ln(k_{obs})$ *vs.* $1/T$ gave an activation energy of 5.6($\pm$0.6) kJ mol$^{-1}$, which is low when compared to the literature value of 45.5 kJ mol$^{-1}$ for $[Ru(bipy)_3]^{2+}$.

Polypyridyl complexes of second and third row transition metal ions such as ruthenium(II), osmium(II), rhenium(I) and iridium(III) have been the focus of attention for many years, particularly in light of their interesting and beneficial electrochemical and photophysical properties.[1–6] Without question the most extensively explored complex is $[Ru(bipy)_3]^{2+}$ (bipy = 2,2′-bipyridyl) which, owing to its relatively long-lived excited state lifetime, readily fluoresces at room temperature in a range of solvents. The photophysical properties of the complex are now generally well understood, with emission occurring from a triplet metal-to-ligand charge-transfer ($^3$MLCT) state which is formulated as $[Ru^{III}(bipy)(bipy^-)]^{2+}$ and in which the promoted electron resides in the LUMO of a single bipy ligand.[7] Luminescence quenching of $[Ru(bipy)_3]^{2+}$ has been extensively studied using diverse reagents, and occurs either *via* oxidative/reductive electron transfer or energy transfer processes.[8] Attempts to harness the beneficial aspect of this quenching have seen the building of secondary binding sites onto the "$Ru(bipy)_3$" core, such as crown ethers,[9] cyclodextrins,[10] azamacrocycles[11] and pH receptive groups for sensing applications.[12–14]

Although a plethora of such luminescent probes exist, detailed studies into their basic photophysical properties often reveal interesting and unexpected results. For instance, Hupp *et al.*[15] observed that contrary to expectation, the excited state lifetime of the complex **1** increased, when a pyridinium group was attached directly to the phenanthroline ligand.

As part of our own research effort into creating exotic photoactive assemblies,[16] we report herein a detailed investigation of the temperature and solvent dependent photophysical properties of a ruthenium(II) polypyridyl complex (**2**) similar to that reported by Hupp. In the case of complex **2**, however, the 4-pyridinium-4′-pyridine group is connected to the metal binding group *via* a methylene spacer and observed solvent effects are considered to occur *via* through-space interactions.

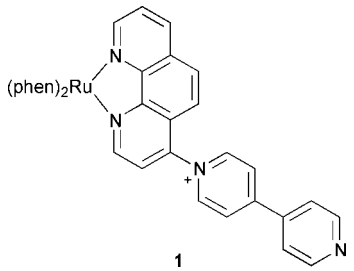


**1**

## Experimental

All bulk chemicals were purchased from Aldrich and used as supplied. Electronic spectra were recorded using a Shimadzu UV-3101PC spectrophotometer. Reference and sample spectra were collected using optically matched 1 cm quartz cuvettes. Corrected spectra were produced by sample-reference subtraction using the en-suite programs. NMR spectra were obtained on a Bruker AM360 360 MHz FT-NMR spectrometer using the Bruker Aspect 3000 suite of programs. All samples were referenced internally to solvent resonances. Steady-state fully corrected luminescence spectra were obtained on a Fluoromax-2 spectrofluorimeter using the en-suite programs. Spectra were obtained in a 1 cm quartz cuvette. Mass spectra were obtained using a JEOL JMS 700 ("The MStation") mass spectrometer. FAB mass spectra were obtained from a sample matrix consisting of the sample and 3-nitrobenzyl alcohol (NOBA). Electrospray mass spectra were measured by the EPSRC Mass Spectrometry Service Centre at Swansea, and typically used a mobile phase of acetonitrile–1% formic acid with cone voltages varying from 20 to 90 V. Nanosecond laser spectroscopic measurements were performed using a Spectron Laser Services SL803 Q-switched Nd YAG solid-state laser operating at 532 nm. The laser pulse duration was 15 ns at an output energy of 800 μJ. Laser energy was monitored using a

 DOI: 10.1039/b007962f

Laser Precision Corporation RM-6600 universal radiometer. Transient luminescence spectra were recorded using an Applied Photophysics photomultiplier, an Applied Photophysics F/3.4 monochromator and a Tektronix TDS520 two channel digitising oscilloscope. All data was analysed using a kinetic fit program.[17] Lifetime values were found to be independent of monitoring wavelength. For time-resolved spectroscopic work the samples were thoroughly purged with $N_2$ for a least 10 minutes.

Emission band-shape analysis was performed using an adaptation of the method reported by Harriman *et al.*[18] Mathematical calculations were performed using the commercial package MATHCAD[19] and processed in a commercial spreadsheet in which simulated and observed spectra were fitted.

### Luminescence quantum yield

Quantum yield of luminescence was calculated by measuring emission intensity over a range of laser powers for optically matched samples of (**2**) and $[Ru(bipy)_3]^{2+}$ as standard (std) ($\Phi = 0.062$), and using the equation: $[\phi(2)/\phi(\text{std})] = [m(\text{std})/m(2)]$, where $m$ = slope of signal intensity *vs.* laser power.[20]

### X-Ray crystallography

Owing to the extremely small size of the crystals, data on $L_1$ and **2** were collected at the CLRC Daresbury Laboratory using station 9.8, which uses high photon fluxes produced by the SRS 5 T wiggler magnet. A Siemens-SMART CCD area detector was used for data collection in combination with the Siemens-SMART suite of programs.[21] Frame integration was achieved by use of the SAINT program[22] and absorption corrections and beam-decay corrections were performed with the SADABS program.[23] The structures were solved by direct methods (SHELXS-97),[24] and refined (SHELXL-97)[24] on $F^2$ using all data. All aliphatic and aromatic C–H hydrogen atoms were included at calculated positions. Relevant crystallographic data pertaining to $L_1$ and **2** are collected in Table 1.

CCDC reference number 440/252. See http://www.rsc.org/suppdata/nj/b0/b007962f/ for crystallographic files in .cif format.

The ligand $L_1$ was prepared according to the literature.[25] Analytical data: $^1$H NMR ($d_6$-acetone): $\delta$ 6.33 (s, 4H), 7.64 (dd, $J = 2.0$, $J' = 5.0$, 2H), 8.00 (dd, $J = 6.2$, $J' = 1.7$, 4H), 8.66 (s, 2H), 8.77 (bd, $J = 7.0$, 4H), 8.80 (d, $J = 5.2$, 2H), 8.87 (d, $J = 6.2$, 4H), 9.51 (d, $J = 7.2$ Hz, 4H). FAB-MS (NOBA matrix): $m/z$ 639 $(M - PF_6)^+$, 493 $(M - 2PF_6)^+$. Anal. calc. for $C_{32}H_{26}N_6P_2F_{12}\cdot H_2O$: C, 47.87; H, 3.52; N, 10.47; found: C, 47.28; H, 3.69; N, 9.87%.

**Table 1** Crystallographic data parameters obtained for compounds $L_1$ and **2**

| Compound | **2** | $L_1$ |
|---|---|---|
| Chemical formula | $C_{52}H_{42}B_4F_{16}N_{10}Ru$ | $C_{32}H_{26}F_{12}N_6P_2$ |
| $M_r$ | 1255.27 | 784.53 |
| Space group | $P\bar{1}$ | $P2_1/n$ |
| Crystal system | Triclinic | Monoclinic |
| $a$/Å | 13.1025(1) | 6.3652(9) |
| $b$/Å | 13.5227(1) | 35.256(11) |
| $c$/Å | 16.4607(1) | 7.6591(17) |
| $\alpha$/° | 94.579(1) | |
| $\beta$/° | 102.822(1) | 108.033(17) |
| $\gamma$/° | 105.621(1) | |
| $V$/Å$^3$ | 2708.3(3) | 1634.4(7) |
| $Z$ | 2 | 2 |
| $\mu$/mm$^{-1}$ | 0.392 | 0.172 |
| Temperature/°C | −113 | −113 |
| No. data collected | 16 321 | 7064 |
| No. unique data | 11 274 | 3091 |
| $R_{int}$ | 0.0264 | 0.0989 |
| Final $R1$ | 0.0473 | 0.0973 |
| Final $R_w^2$ | 0.1193 | 0.1556 |

### Preparation of $[Ru(bipy)_2L_1](PF_6)_2$ (2)

Compound $L_1$ (375 mg, 0.48 mmol) and Λ-*cis*-[Ru(bipy)$_2$(pyridine)$_2$][(+)-*O*,*O*′-dibenzoyl-L-tartrate] (450 mg, 0.46 mmol) were added to ethylene glycol (12 ml, 10% distilled water) in a 25 ml round-bottomed flask. The reaction mixture was stirred and heated to 120 °C for four hours before being cooled to room temperature and diluted with distilled water (18 ml). The resultant solution was then filtered and a saturated aqueous solution of ammonium hexafluorophosphate was added dropwise to the filtrate until no further precipitation was observed. The solid was collected by filtration and washed with distilled water. The material was then purified by column chromatography [$SiO_2$, MeOH–2N $NH_4Cl$–$MeNO_2$ (7 : 2 : 1)]. Yield 425 mg, 62%. $^1$H NMR ($d_6$-acetone): $\delta$ 6.28 (s, 4H), 7.55 (m, 4H), 7.65 (d, $J = 5.7$, 2H), 7.96–7.98 (m, 4H), 8.01 (m, 4H), 8.11 (d, $J = 5.8$, 2H), 8.19 (m, 4H), 8.62 (d, $J = 6.4$, 4H), 8.75–8.81 (m, 6H), 8.90 (m, 4H), 9.28 (d, $J = 6.3$ Hz, 4H). FAB-MS (NOBA matrix) and Electrospray MS: $m/z$ 1343 $(M - PF_6)^+$, 1197 $(M - 2PF_6)^+$, 1052 $(M - 3PF_6)^+$. Anal. calc. for $C_{56}H_{52}N_{10}P_4F_{24}Ru$: C, 43.02; H, 3.35; N, 8.96; found: C, 42.86; H, 3.14; N, 9.05%.

## Results and discussion

### Synthesis

The synthesis of $L_1$ is depicted in Scheme 1 and is a precursor in the manufacture of more elaborate catenane and cyclophane derivatives.[16] Synthesis of the ruthenium complex was carried out by refluxing $L_1$ in an ethylene glycol–water mixture with one equivalent of Λ-*cis*-[Ru(bipy)$_2$(pyridine)$_2$]-[(+)-*O*,*O*′-dibenzoyl-L-tartrate].[26] As well as forming the desired complex (**2**), a number of other side products were obtained, as evidenced by thin layer chromatography. These other products are attributed to larger aggregates formed by complexation of the ruthenium(II) to the "free" nitrogen of the pyridyl groups. By careful column chromatography [silica gel, MeOH–2N $NH_4Cl$–$MeNO_2$ (7 : 2 : 1)] the desired compound (**2**) was separated from all other side products in a reasonable (62%) yield. The by-products have not yet been fully characterized.

### Structural analysis

The low-energy conformation of uncomplexed ligands based on bipy is normally described as *transoid* where the two nitrogens are *anti* to each other. This geometry is attributed to unfavourable electrostatic repulsion between the lone pairs on the nitrogens, which forces the pyridine rings as far apart as possible. The molecular structure of precursor ligand $L_1$ demonstrates this point.

When complexed to the "Ru(bipy)$_2$" unit, the ligand $L_1$ is, as expected, forced into the *cisoid* conformation, as shown in Fig. 1. The torsion angle between the nitrogen atoms of the 2,2′-bipyridyl group is only *ca.* 2°.

The coordination geometry around the ruthenium ion is a distorted octahedron, from inspection of the selected bond lengths and angles collected in Table 2. The average Ru–N bond distance is 2.06 Å, typical for bipyridyl complexes of dicationic ruthenium.[27] As observed in the precursor ligand $L_1$, the two rings of the *N*-methylene-4-pyridinium-4′-pyridine moieties are non-coplanar with torsion angles of *ca.* 12 (C124–C123–C133–C134) and 25° (C144–C143–C153–C152). This indicates a lack of double-bond character in the central C–C bond joining the two pyridine groups and, therefore, supports the hypothesis that, at least in the ground state, there is no

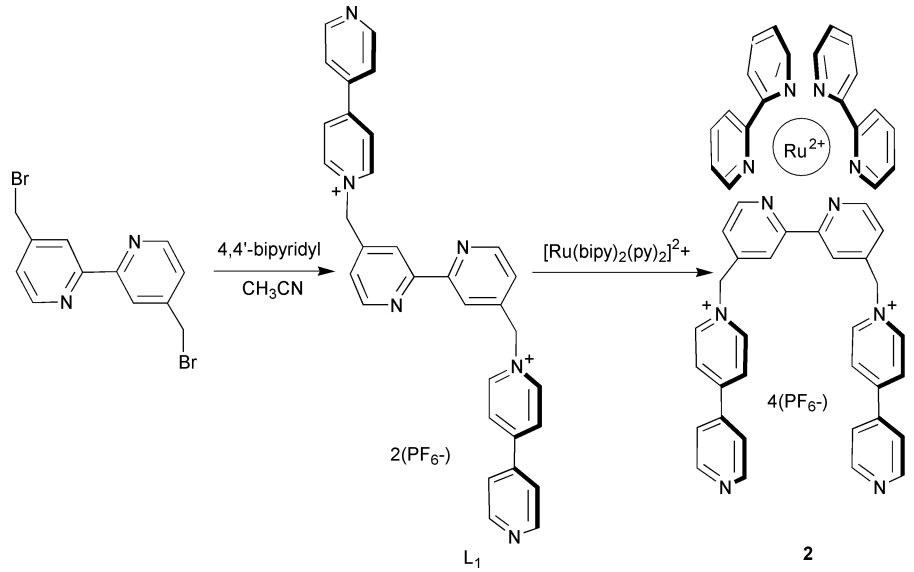


**Scheme 1** Procedures used in the preparation of complex **2**.

electron migration from the "free" nitrogen to the electron deficient cationic nitrogen. Furthermore, the two "free" nitrogen ends of the *N*-methylene-4-pyridinium-4′-pyridine units are well separated (*ca.* 6.5 Å), which suggests that these two groups do not interact with one another. When discussing the photophysical properties of complex **2**, it is thus reasonable to treat each bipyridinium arm of the complex as an independent unit. The methylene units which connect the bipy and 4-pyridinium-4′-pyridine groups are almost tetrahedral in geometry (C113–C2–N140 108.6, C103–C1–N120 108.9°) and, as a result, the closest contact distance between the quaternary pyridinium nitrogen (N140) and bipy ligand (C113) is only *ca.* 2.4 Å. This arrangement is indeed close enough to support a through-space interaction of the two groups, especially in the excited-state, in which an electron is located in the LUMO of the bipy group.

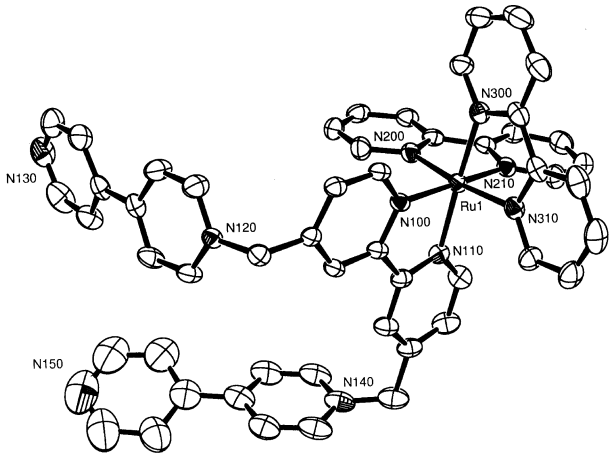


**Fig. 1** Side-on view of the molecular complex **2**. Tetrafluoroborate anions are omitted for clarity of presentation.

**Table 2** Selected bond distances and angles observed for complex **2**

| | Bond length/Å | | Bond angle/° |
|---|---|---|---|
| Ru(1)–N(100) | 2.047(3) | N(100)–Ru(1)–N(210) | 172.32(12) |
| Ru(1)–N(210) | 2.053(3) | N(110)–Ru(1)–N(300) | 173.31(13) |
| Ru(1)–N(110) | 2.049(3) | N(310)–Ru(1)–N(200) | 173.69(12) |
| Ru(1)–N(300) | 2.056(3) | N(100)–Ru(1)–N(200) | 95.03(12) |
| Ru(1)–N(200) | 2.060(3) | N(100)–Ru(1)–N(110) | 79.26(12) |
| Ru(1)–N(310) | 2.064(3) | N(100)–Ru(1)–N(300) | 97.12(12) |

## Photophysical properties

The absorption and fully-corrected luminescence profiles of complex **2** and $[Ru(bipy)_3]^{2+}$ in acetonitrile for comparison are illustrated in Fig. 2. Complex **2** exhibits the characteristic MLCT absorption band centred at 22 124 $cm^{-1}$ and a corresponding luminescence band centred at 14 822 $cm^{-1}$. The calculated Stokes' shift is 7302 $cm^{-1}$. It is evident that the MLCT absorption band for **2** is considerably broader than that of $[Ru(bipy)_3]^{2+}$. This increased bandwidth is attributed to the existence of another underlying MLCT state which must be associated with the functionalized bipy unit (see later). The overall lower in energy emission band of **2** is a consequence of introduction of the electron withdrawing *N*-methylene-4-pyridinium-4′-pyridine cation onto the bipy backbone. In view of this, the MLCT state is formulated as $[Ru^{III}(bipy)_2(L_1^-)]^{2+}$, but with the electron residing on the bipy portion of the functionalized ligand. Further delocalization of the electron onto the *N*-methylene-4-pyridinium-4′-pyridine segment to generate an extended superligand is discounted, since the connecting methylene will act as an insulator. Furthermore, electron transfer to the *N*-methylene-4-pyridinium-4′-pyridine cation is also unlikely, since this process is thermodynamically unfavourable by *ca.* 0.3 eV.[28]

The luminescence profile of **2** was satisfactorily simulated using eqn. 1 and is depicted in Fig. 3.

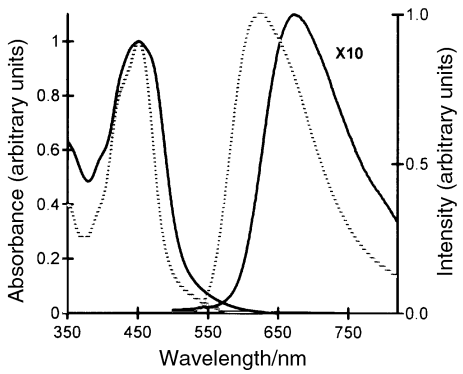


**Fig. 2** Absorption and fully corrected luminescence spectra of complex **2** (dark line) and $[Ru(bipy)_3]^{2+}$ (dashed line) in acetonitrile at 22 °C.

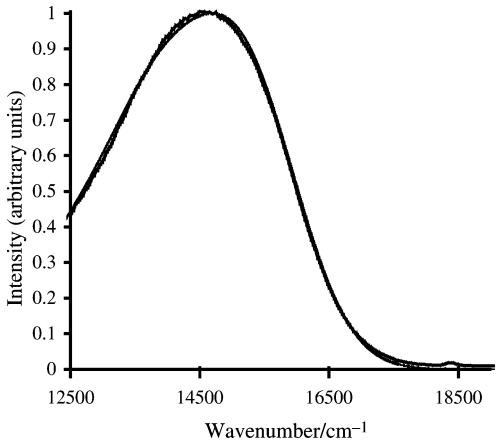


**Fig. 3** Normalized emission spectrum of complex **2** in acetonitrile at 22 °C (solid line) and spectrum simulated using eqn. 1 shown in text (dashed line).

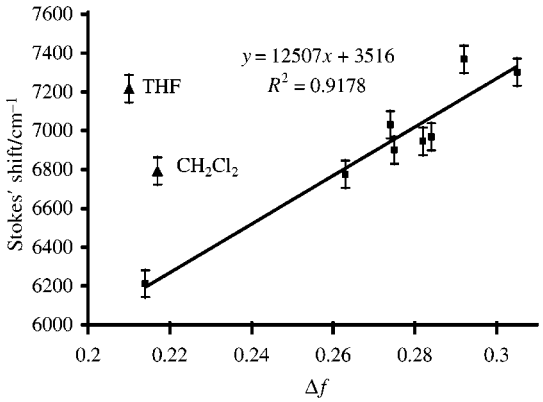


**Fig. 4** Plot of Stokes' shift *vs.* solvent polarity function $\Delta f$ for complex **2** in a range of solvents at 22 °C. Insert shows least-squares straight line fit to data points and goodness-of-fit parameter.

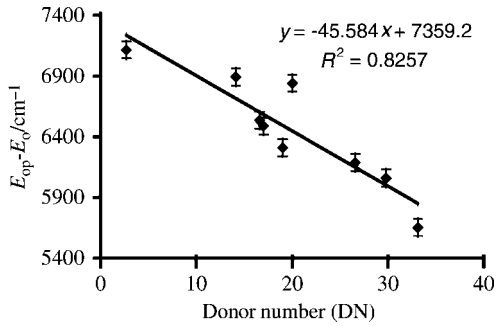


**Fig. 5** Plot of $(E_{op} - E_o)$ *vs.* Gutmann's solvent donor number for complex **2**. Insert shows least-squares straight line fit to data points and goodness-of-fit parameter.

$$I(E) = \sum_{v=0}^{N} \left(\frac{E_o - v\hbar\omega_m}{E_o}\right)^3 \left(\frac{(S_m)^v}{v!}\right) \times \exp\left[-4\ln(2)\left(\frac{E - E_o + v\hbar\omega_m}{v_{1/2}}\right)^2\right] \quad (1)$$

where $I$ = intensity at wavenumber $E$, $E_o$ = energy difference between 0,0 vibronic levels, $\hbar\omega_m$ = medium frequency vibrational mode, $S_m$ = Huang–Rhys electron-vibrational coupling constant and $v_{1/2}$ = half-height band width. In this and other calculations, a good fit was obtained using $N = 10$.

## Solvent effects

It is well established that solvent can play a key role in influencing the absorption and emission spectra of ruthenium polypyridyl complexes.[29,30] In the early work of Meyer *et al.*,[31] solvatochroism displayed by complexes such as $[Ru(NH_3)_5(dmapy)]^{2+}$, where dmapy is 4-(dimethylamino) pyridine, was attributed to solvent hydrogen-bonding to the ammine ligands. In this example, the MLCT absorption band maximum correlated well with the Gutmann solvent donor number (DN).[32] On the other hand, correlation between solvent acceptor number (AN)[31] and absorption/emission spectra of $[Ru(bipy)_2(CN)_2]$ and $[Ru(phen)_2(CN)_2]$ explains their solvatochroism properties, which arise from solvent interaction with the cyanide.[33,34] In all these cases, the ligand which leads to the observed solvatochromic effects is directly attached to the metal ion centre and, thus, would be expected to affect the electronic properties of the complex. The influence of solvent on the electronic properties of complex **2** was expected, at first, to be similar to $[Ru(bipy)_3]^{2+}$, since the appended *N*-methylene-4-pyridinium-4′-pyridine cation and bipy units are decoupled.[35] Thus, absorption and luminescence spectra were recorded for **2** in a range of solvents with varying DN, AN and polarity, and are collected in Table 3. Also summarized are the parameters obtained from band-shape analysis and fitting of the emission spectra using eqn. 1.

## Solvent polarity effects

The solvent effect on an absorption spectrum is governed by the equilibrium ground state and the Frank–Condon excited state, whilst the luminescence spectrum depends upon the equilibrium excited state and the Frank–Condon ground state. To this end, the solvent polarity factor, $(\Delta f)$ introduced by Mataga *et al.*[36,37] and Lippert[38] and used by other workers,[39,40] establishes a means to quantify the Stokes' shift (SS, in $cm^{-1}$) (eqns. 2 and 3) with the change in dipole moment between ground state ($\mu_g$) and excited state ($\mu_e$), induced by alterations in dipole–dipole interactions of the solvent and solute.

**Table 3** Solvent dependent parameters recorded for complex **2** at 22 °C in aerated samples

| Solvent | $E_{op}$[a]/cm$^{-1}$ | $E_{em}$[b]/cm$^{-1}$ | Stokes' shift[c]/cm$^{-1}$ | $E_o$[d]/cm$^{-1}$ | $v_{1/2}$[e]/cm$^{-1}$ | $\hbar\omega_m$[f]/cm$^{-1}$ | $S_m$ |
|---|---|---|---|---|---|---|---|
| $CH_3CN$ | 22 124 | 14 822 | 7302 | 15 232 | 1950 | 1383 | 1.11 |
| $CH_2Cl_2$ | 22 173 | 15 380 | 6793 | 15 793 | 1950 | 1357 | 0.84 |
| $(CH_3)_2CO$ | 21 905 | 14 936 | 6969 | 15 418 | 1950 | 1353 | 0.95 |
| $(CH_3)_2SO$ | 21 834 | 15 058 | 6776 | 15 775 | 2100 | 1543 | 1.20 |
| DMF[g] | 21 786 | 14 755 | 7031 | 15 599 | 2040 | 1312 | 1.30 |
| BuCN[h] | 21 978 | 15 077 | 6901 | 15 442 | 1950 | 1416 | 0.78 |
| $CH_3NO_2$ | 22 026 | 14 657 | 7369 | 14 911 | 1990 | 1446 | 0.69 |
| THF[i] | 21 930 | 14 713 | 7217 | 15 089 | 2050 | 1212 | 0.80 |
| Pyridine | 21 787 | 15 574 | 6213 | 16 135 | 1820 | 1449 | 1.11 |
| Formamide | 21 978 | 15 032 | 6946 | 15 683 | 2005 | 1331 | 1.05 |

[a] Parameters as described in text. ±50 $cm^{-1}$. [b] ±50 $cm^{-1}$. [c] ±100 $cm^{-1}$. [d] ±50 $cm^{-1}$. [e] ±20 $cm^{-1}$. [f] ±20 $cm^{-1}$. [g] *N*,*N*-Dimethylformamide. [h] Butyronitrile. [i] Tetrahydrofuran.

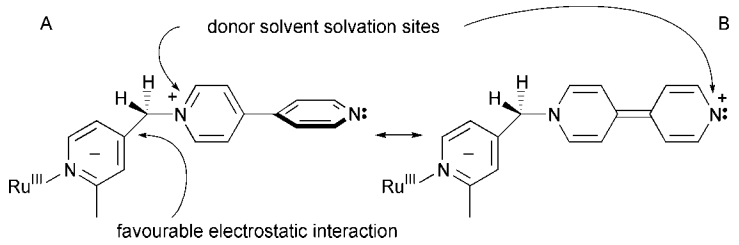


**Scheme 2** Simplified excited-state diagram for **2**.

$$SS = \frac{2}{hc}\Delta f \frac{(\mu_e - \mu_g)^2}{a^3} \quad (2)$$

$$\Delta f = \left(\frac{D-1}{2D+1}\right) - \left(\frac{n^2-1}{2n^2+1}\right) \quad (3)$$

Here $a$ = effective spherical radius (Å), $D$ = static dielectric constant and $n$ = refractive index.[41]

As illustrated in Fig. 4, there is a good correlation between SS and $\Delta f$ for the aprotic solvents of $D > 10$, with SS increasing as solvent polarity increases.[42] The strong solvent dependence of **2** in aprotic media supports a considerable dielectric reorganization of the solvents and is in accord with similar results observed for $[Ru(bipy)_2(CN)_2]$. By using the slope shown in Fig. 5, the change in dipole moment $(\mu_e - \mu_g)$ was calculated[43] using $a \approx 4.4$ Å to be *ca.* 10 *D*, which is approximately half the theoretical calculated value. A lower than expected value fits with previous work on related systems and attributed to electron delocalization and polarization of the ligand electrons.[30]

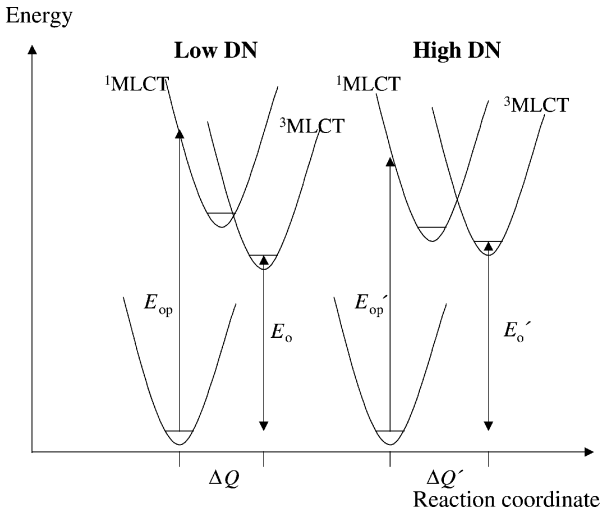


**Fig. 6** A simplified potential-energy surfaces diagram for **2** in a solvent of low and high donor number.

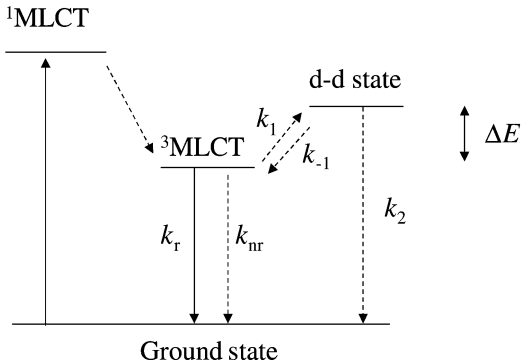


**Fig. 7** Excited-state deactivation model for ruthenium(II) polypyridyl complexes. The meaning of symbols is explained in the text.

### Solvent donor number

Meaningful relationships between Gutmann's solvent number AN and parameters for **2** could not be obtained. Dependence of absorption/emission data and calculated parameters obtained using eqn. 1 (Table 3) on Gutmann's DN were, however, noticeable. It was observed that with increasing DN, values of emission maximum ($E_{em}$) and $E_o$ increased whilst, in contrast, the absorption maximum ($E_{op}$) values decreased. A satisfactory linear correlation between $(E_{op} - E_o)$ and DN is illustrated in Fig. 5, and indicates that the energy difference between the first-excited $^1$MLCT and $^3$MLCT states decreases with increasing DN.

Although less clear cut, it was also found that the calculated Huang–Rhys ($S_m$)[44] values did also gradually increase with increasing DN. Since $S_m$ is related to the equilibrium configurations of the ground and excited states by the dimensionless fractional displacement parameter ($\Delta_j$) (eqns. 4 and 5), this suggests that the structure of the acceptor ligand in the complex does change slightly depending on the donor ability of the solvent. Furthermore, since the extent of mixing between ground and excited state will decrease, there will be a greater degree of charge transfer to the acceptor ligand in the excited state.[45,46]

$$S_m = \tfrac{1}{2}\Sigma_j \Delta_j^2 \quad (4)$$

$$\Delta_j = (Q_o^g - Q_o^e)(m\varpi_j/\hbar)^{1/2} \quad (5)$$

where $m$ = reduced mass and $Q_o^e$ and $Q_o^g$ represent the excited and ground state equilibrium positions, respectively.

### Nature of solvent–solute interaction

It is clear that solvent donation to complex **2** must occur at an electron deficient acceptor site. In view of this, the cationic nitrogen of the *N*-methylene-4-pyridinium-4′-pyridine group is a likely interaction location, and two cationic resonance forms can exist, as illustrated in Scheme 2. Since in the excited state an electron resides on the bipy segment, the resonance form **A** would be the more favoured by a simple electrostatic argument, and in keeping with the X-ray crystal structure (Fig. 1). Preferential solvent donation to the resonance form **A** would therefore lead to a reduction in positive charge at the nitrogen, and a diminution in stabilisation of the excited state. Thus, with increasing DN, it is expected that the excited state would rise in energy. Unfortunately, the effect of the solvent on the ground state is less clear cut.

### Potential energy surface model

In order to incorporate all the previous results, a simplified potential energy surface diagram can be constructed which

encompasses changes due to solvent donation (Fig. 6). A particularly critical key feature of the model is worth noting: in order to increase $E_o$ with DN whilst concomitantly allowing a decrease in $E_{op}$, there has to be an increase in energy of the $^3$MLCT state coupled to a lowering in energy of the $^1$MLCT state. As well as this, it is also noted that, with respect to the $^3$MLCT state, $\Delta Q' > \Delta Q$ to account for structural alteration in the acceptor ligand.

### Temperature dependency studies

The observed rate constant ($k_{obs}$) for decay of the excited state in $[Ru(bipy)_3]^{2+}$ over a modest temperature range can be fitted to a three term expression (eqn. 6), which is pictorially depicted in Fig. 7.

$$k_{obs} = k_{nr} + k_r + A' \exp\left(\frac{-\Delta E}{RT}\right) \quad (6)$$

where $k_{obs}$ = observed rate constant for excited state decay, $k_{nr}$ = non-radiative decay constant, $k_r$ = radiative decay constant, $A'$ = pre-exponential factor associated with deactivation from the d–d state and $\Delta E$ = activation energy. Because of the thermally-activated deactivation process, the Arrhenius plot for $[Ru(bipy)_3]^{2+}$ is typically curved over the range 233 to 303 K affording a $\Delta E$ value in acetonitrile of 3800 cm$^{-1}$.[35]

The Arrhenius plot for **2** in acetonitrile over the temperature range 274 to 333 K is illustrated in Fig. 8. The lack of curvature to the plot suggests that the model shown in Fig. 8 is not applicable. Indeed, the $\Delta E$ value as calculated from the least-squares fit to the gradient is only 464 $\pm$ 10 cm$^{-1}$, with a corresponding pre-exponential factor ($A$) of 3.5 $\times$ 10$^7$ s$^{-1}$.

As depicted in Fig. 7 the deactivation of the MLCT state *via* the d–d excited state can be explained in terms of three competing processes, such that:

$$k' = k_1\left(\frac{k_2}{k_{-1} + k_2}\right) \text{ where } k' = A' \exp\left(\frac{-\Delta E}{RT}\right) \quad (7)$$

It is clear that a number of cases exist depending on the relative values of the three rate constant terms. In the first case scenario, $k_{-1} \gg k_2$ so that $k' = (k_1/k_{-1})k_2$ and the MLCT and d–d state are in equilibrium. Alternatively, $k_{-1} \ll k_2$ such that $k' = k_1$ and the pre-exponential term is representative of the MLCT to d–d crossover. In reported cases of ruthenium(II) complexes, the first two limiting cases have been identified. For systems where $k_{-1} \gg k_2$ the ($A$) value is typically 10$^9$–10$^{10}$ s$^{-1}$ and $\Delta E$ is *ca.* 2000 cm$^{-1}$. In the second case ($k_{-1} \ll k_2$) and, as observed for $[Ru(bipy)_3]^{2+}$, $\Delta E$ is in the range 3000–4000 cm$^{-1}$ with a pre-exponential value in the order of 10$^{12}$–10$^{14}$ s$^{-1}$.[35] It is evident that the data for **2** do not fit to any of these two cases. Using the $k_{obs}$ value at 298 K of 3.8 $\times$ 10$^6$ s$^{-1}$ and the quantum yield of luminescence ($\phi_f$) of 0.0092 for **2**, the corresponding $k_r$ value was calculated (eqn. 8) as 3.5 $\times$ 10$^4$ s$^{-1}$. For comparison, the corresponding $k_r$ value for $[Ru(bipy)_3]^{2+}$ is 7.7 $\times$ 10$^4$ s$^{-1}$.[35] Using the $k_r$ value for **2** the total non-radiative rate constant ($k_{tnr}$) (eqn. 9) is thus 3.8 $\times$ 10$^6$ s$^{-1}$.

$$k_r = \phi_f k_{obs} \quad (8)$$

$$k_{tnr} = k_{obs} - k_r \quad (9)$$

### Deactivation model

The general deactivation model for ruthenium(II) polypyridyl complexes is best illustrated using two intersecting parabolas, as shown in Fig. 9, and in which the abscissa represents a ligand-based vibration. Since the Ru–N bond lengths in **2** are very similar to analogous ruthenium(II) polypyridyl complexes, it is reasonable to assume that the energy of the d–d state is also comparable. On the other hand, the luminescent MLCT state in **2** is lower in energy by *ca.* 1300 cm$^{-1}$, since its emission profile is red-shifted, and not necessarily identical in character to the $[Ru(bipy)_3]^{2+}$ MLCT state. In general, for simple ruthenium(II) bipy–based complexes, $k_{nr}$ varies linearly with emission energy, such that rapid non-radiative deactivation occurs when the energy of the excited state is low. It is also known that, as the energy of the MLCT decreases, the barrier $\Delta E$ gets larger so that excited state deactivation is not controlled by the thermally activated d–d state. It is evident that lowering the $^3$MLCT potential energy surface in Fig. 9A would result in an increase in $\Delta E$. This conundrum, however, can be adequately explained if we assume that the calculated $\Delta E$ value does not correspond to the MLCT-d–d activation barrier. Since the MLCT emission band for **2** is lower in energy compared to $[Ru(bipy)_3]^{2+}$, the actual $\Delta E$ value should be *ca.* 5100 cm$^{-1}$ which affords a $k'$ value of only 2.1 $\times$ 10$^3$ s$^{-1}$.[47] Thus, for **2** the contribution to non-radiative deactivation *via* the d–d state is insignificant and all deactivation occurs *via* the MLCT state.[48] In the circumstance of **2** $\Delta E$ is associated with the thermal population of another higher-lying MLCT state (Fig. 9B), which is both consistent with the lower symmetry of the complex and the broad emission band. Overall, the general excited state behaviour of **2** is consistent

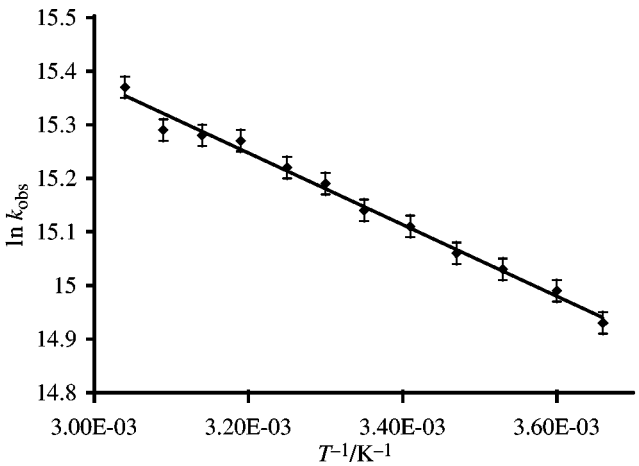


**Fig. 8** Arrhenius plot of ln $k_{obs}$ *vs.* $1/T$ for **2** in acetonitrile.

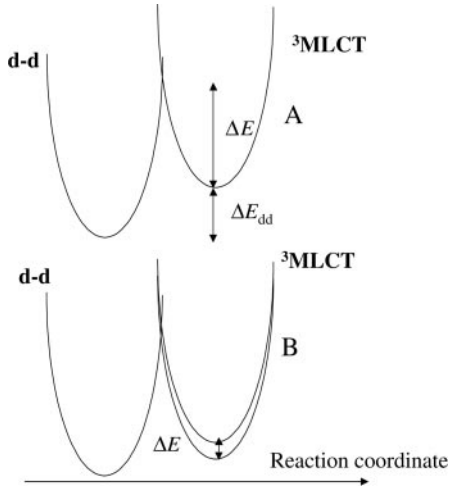


**Fig. 9** MLCT and d–d potential energy surfaces for a ruthenium(II) polypyridyl complex showing the relationship between $\Delta E$, $\Delta E_{dd}$ and reaction coordinate. The cases A and B are discussed in the text.

with a ruthenium bipy-based complex in which the appended unit does not contribute by way of a rotational mechanism to excited-state deactivation. The observed low emission from **2** is consistent with efficient non-radiative deactivation, as predicted by the energy-gap law.

## Conclusions

The detailed photophysical study of complex **2** has revealed that strongly electron donating solvents can both perturb the energy of the emitting $^3$MLCT state and the structure of the acceptor ligand. Solvent interaction is envisaged to occur at the appended *N*-methylene-4-pyridinium-4′-pyridine unit, which is connected to the metal binding bipy group *via* a saturated methylene spacer. Perturbation of the $^3$MLCT state is thus proposed to occur by way of a through-space dipole–dipole interaction. This result would suggest that judiciously positioned, yet connected *via* saturated linkers, electron deficient groups can play a significant role in controlling the photophysical behaviour of ruthenium(II) polypyridyl complexes.

## Acknowledgements

This work was supported by the University of Glasgow (A. C. B., L. J. F.), the University of Paisley (A. J. M.) and the Physical Sciences Research Council, EPSRC, (P. R. M., G. S., S. J. T.). We would also like to thank the EPSRC Mass Spectrometry Service Centre at Swansea for use of the electrospray service.

## References and notes

1 V. Balzani, S. Campagna, G. Denti, A. Juris, S. Serroni and M. Venturi, *Acc. Chem. Res.*, 1998, **31**, 26.
2 E. C. Constable, *Chem. Commun.*, 1997, 1073.
3 A. Harriman and R. Ziessel, *Chem. Commun.*, 1996, 1707.
4 M. R. Waterland, T. J. Simpson, K. C. Gordon and A. K. Burrell, *J. Chem. Soc., Dalton Trans.*, 1998, 185.
5 R. E. Holmlin, J. A. Yao and J. K. Barton, *Inorg. Chem.*, 1999, **38**, 174.
6 K. Kalyanasundaram, *Photochemistry of Polypyridine and Porphyrin Complexes*, Academic Press, London, 1992.
7 R. F. Dallinger and W. H. Woodruff, *J. Am. Chem. Soc.*, 1979, **101**, 4391.
8 G. J. Kavarnos, *Fundamentals of Photoinduced Electron Transfer*, VCH Publishers, Inc., Weinheim, 1993.
9 P. D. Beer, O. Kocian, R. J. Mortimer and C. Ridgway, *J. Chem. Soc., Faraday Trans.*, 1993, **89**, 333.
10 D. Armspach, D. Matt and A. Harriman, *Eur. J. Inorg. Chem.*, 2000, **6**, 1147.
11 A. M. Josceanu, P. Moore and P. Sheldon, *Rev. Roum. Chim.*, 1998, **43**, 945.
12 B. Geisser, A. Ponce and R. Alsfasser, *Inorg. Chem.*, 1999, **38**, 2030.
13 A. Del Guerzo, A. K.-D. Mesmaeker, M. Demeunynck and J. Lhomme, *J. Phys. Chem. B*, 1997, **101**, 7012.
14 M. Guardigli, L. Flamigni, F. Barigelletti, C. S. W. Richards and M. D. Ward, *J. Phys. Chem.*, 1996, **100**, 10620.
15 C. Berg-Brennan, P. Subramanian, M. Absi, C. Stern and J. T. Hupp, *Inorg. Chem.*, 1996, **35**, 3719.
16 A. C. Benniston, P. R. Mackie and A. Harriman, *Angew. Chem., Int. Ed.*, 1998, **39**, 354.
17 KINFIT, Kinetic fitting program, On Line Instrument Systems, 1989.
18 A. Harriman, F. M. Romero, R. Ziessel and A. C. Benniston, *J. Phys. Chem. A*, 1999, **103**, 5399.
19 MATHCAD, Mathematical calculations program, MathSoft Inc., 1986–1995, Cambridge, MA.
20 This method is an adaptation of that used in the measurement of singlet oxygen quantum yield, see: M. A. J. Rogers and P. T. Snowden, *J. Am. Chem. Soc.*, 1982, **104**, 5541. The steady-state method using the integration of the luminescence profile for optically matched samples of **2** and $[Ru(bipy)_3]^{2+}$ in $CH_3CN$ gave similar results.
21 SMART, Program for area detector data collection, Siemens Analytical X-Ray Instruments Inc., Madison, WI, USA, 1996.
22 SAINT, Program for area detector absorption correction, Siemens Analytical X-Ray Instruments Inc., Madison, WI, USA, 1996.
23 G. M. Sheldrick, SADABS, Program for Siemens Area Detector Absorption Correction, University of Göttingen, Germany, 1996.
24 G. M. Sheldrick, SHELXS-97, SHELX-97 (release 97-2), Programs for crystal structure analysis, University of Göttingen, Germany, 1997.
25 A. C. Benniston, P. R. Mackie and A. Harriman, *Tetrahedron Lett.*, 1997, **38**, 3577.
26 X. Hau and A. von Zelewsky, *Inorg. Chem.*, 1995, **34**, 5791.
27 D. P. Rillema, D. S. Jones, C. Woods and H. A. Levy, *Inorg. Chem.*, 1992, **31**, 2935.
28 Calculated using equations from ref. 15 and $E(Ru^{2+}/Ru^{3+}) = 1.27$ eV, $E(py^{+/0}) = -0.90$ and $E_o = 1.9$ eV.
29 N. S. Hush and J. R. Reimers, *Coord. Chem. Rev.*, 1998, **177**, 37.
30 B. S. Brunschwig, C. Cruetz and N. Sutin, *Coord. Chem. Rev.*, 1998, **177**, 61.
31 J. C. Curtis, B. P. Sullivan and T. J. Meyer, *Inorg. Chem.*, 1983, **22**, 224.
32 U. Mayer, *Pure Appl. Chem.*, 1979, **51**, 1697.
33 N. Kitamura, M. Sato, H.-B. Kim, R. Obata and S. Tazuke, *Inorg. Chem.*, 1988, **27**, 651.
34 P. Belser, A. von Zelewsky, A. Juris, F. Barigelletti and V. Balzani, *Gazz. Chim. Ital.*, 1985, **115**, 723.
35 J. V. Caspar and T. J. Meyer, *J. Am. Chem. Soc.*, 1983, **105**, 5583.
36 N. Mataga, Y. Kaifu and M. Koizumi, *Bull. Chem. Soc. Jpn.*, 1955, **28**, 690.
37 N. Mataga, Y. Kaifu and M. Koizumi, *Bull. Chem. Soc. Jpn.*, 1956, **29**, 465.
38 E. Lippert, *Z. Naturforsch., A: Astrophys. Phys. Phys. Chem.*, 1955, **10**, 541.
39 J. Cortés, H. Heitele and J. Jortner, *J. Phys. Chem.*, 1994, **98**, 2527.
40 M. Muruyama, H. Matsuzawa and Y. Kaizu, *Inorg. Chem.*, 1995, **34**, 3232.
41 Values of *D* and *n* taken from: S. L. Murov, I. Carmichael and G. L. Hug, *Handbook of Photochemistry Vol. 2*, Marcel Dekker, New York, 1993, p. 283.
42 H-bonding solvents are excluded, since these may interact with the "free" nitrogen and hence alter the electron distribution within the *N*-methylene-4-pyridinium-4′-pyridine cation.
43 Calculated using $\mu_e - \mu_g = 0.010\sqrt{ma^3}$ where $m$ = slope ($cm^{-1}$). Taken from ref. 38.
44 J. V. Caspar, T. D. Westmoreland, G. H. Allen, P. G. Bradley, T. J. Meyer and W. H. Woodruff, *J. Am. Chem. Soc.*, 1984, **106**, 3492.
45 K. R. Barqawi, Z. Murtaza and T. J. Meyer, *J. Phys. Chem.*, 1991, **95**, 47.
46 G. A. Mines, J. A. Roberts and J. T. Hupp, *Inorg. Chem.*, 1992, **31**, 125.
47 The new $\Delta E$ value is assumed to be 3800 $cm^{-1}$ ($[Ru(bipy)_3]^{2+}$) + 1300 $cm^{-1}$ (energy difference in emission energies) and $A' \approx 10^{14}$ $s^{-1}$.
48 This point is further supported since, for a ruthenium(II) bipy-based complex with an emission energy of 14 822 $cm^{-1}$, the $k_{nr}$ value would be *ca.* $2 \times 10^6$ $s^{-1}$ (see ref. 35), which is comparable to the $k_{nr}$ value calculated for **2**.